Cancer Chemother Pharmacol (2012) 69:911–921
DOI 10.1007/s00280-011-1740-7

ORIGINAL ARTICLE

A novel multi-targeted tyrosine kinase inhibitor, linifanib (ABT-869), produces functional and structural changes in tumor vasculature in an orthotopic rat glioma model

Yanping Luo · Fang Jiang · Todd B. Cole · Vincent P. Hradil · David Reuter · Arunava Chakravartty · Daniel H. Albert · Steven K. Davidsen · Bryan F. Cox · Evelyn M. McKeegan · Gerard B. Fox

Received: 1 February 2011 / Accepted: 6 September 2011 / Published online: 12 November 2011

Abstract Tyrosine kinase inhibitors represent a class of targeted therapy that has proven to be successful for cancer treatment. Linifanib is a novel, orally active multi-targeted receptor tyrosine kinase (RTK) inhibitor that exhibits potent antitumor and antiangiogenic activities against a broad spectrum of experimental tumors and malignancies in patients. The compound is currently being evaluated in phase 2 and 3 clinical trials. To investigate the effectiveness of linifinib against gliomas and the mechanism of drug action, we characterized treatment-induced antitumor and antiangiogenic responses to linifanib in an orthotopic rat glioma model. The effect of linifanib treatment on tumor growth was determined by tumor volume assessment using anatomical magnetic resonance imaging (MRI). Changes in tumor microvessel function were evaluated with dynamic contrast-enhanced MRI (DCE-MRI). Immunohistochemistry (IHC) was applied to excised tumor samples to examine underlying changes in vascular structures and target receptor expression. Linifanib (10 mg/kg) given twice daily inhibited tumor growth following treatment for 7 days with tumor volumes being 149 ± 30 and 66 ± 7 mm^3 for vehicle-and linifanib-treated groups, respectively. A significant reduction of 37 ± 13% in tumor perfusion and microvessel permeability (measured by K^{trans}) was observed as early as 2 h after administration compared with vehicle treatment. Continuous linifanib administration further reduced K^{trans} at later time points until the end of the study (7 days post-treatment). At day 7, K^{trans} was reduced by 75 ± 32% for linifanib treatment compared with vehicle treatment. Significant reduction in total blood vessel density and improved vessel wall integrity were observed, and staining for target receptor expression confirmed inhibition of phospho VEGFR-2 and PDGFR-β by linifanib treatment. These results demonstrate significant antitumor and antiangiogenic activity against gliomas by linifanib, a property that may result from the inhibition of VEGFR-2 and PDGFR-β-mediated vascular changes. DCE-MRI measured K^{trans} changes at early treatment stages may be a useful pharmacodynamic marker for linifanib activity in clinical trials, and basal K^{trans} may provide predictive value for tumor progression.

Keywords Glioma · Blood vessel · Angiogenesis · Perfusion · Permeability · Linifanib · DCE-MRI

Y. Luo · T. B. Cole · V. P. Hradil · B. F. Cox · G. B. Fox
Advanced Technology, Global Pharmaceutical Research and Development, Abbott Laboratories, Abbott Park, IL, USA

Y. Luo (✉)
Department R4DF, Abbott Laboratories, Building AP4A-1, 100 Abbott Park Road, Abbott Park, IL 60064, USA
e-mail: yanping.luo@abbott.com

F. Jiang · D. Reuter · D. H. Albert · S. K. Davidsen · E. M. McKeegan
Cancer Research, Global Pharmaceutical Research and Development, Abbott Laboratories, Abbott Park, IL, USA

A. Chakravartty
Exploratory Statistics, Global Pharmaceutical Research and Development, Abbott Laboratories, Abbott Park, IL, USA

Introduction

Sustained angiogenesis is required for the growth of all solid cancers. Signaling through the vascular endothelial growth factor receptor (VEGFR) family plays a key role in angiogenesis and other processes necessary for tumor progression [12]. Targeting VEGF/VEGFR signaling has been proven an effective antiangiogenic approach for

cancer treatment [9]. The platelet-derived growth factor receptor (PDGFR) family includes several compelling anticancer targets that are also involved in angiogenesis and play important roles in maintaining blood vessel structure. Functional disruption of PDGFR-β leads to a lack of pericytes, resulting in severe vascular defects [3, 7]. Microvessels (MV) lacking pericyte coverage are sensitized to deprivation of VEGF signaling [3, 20]. It has been shown in preclinical studies that simultaneous inhibition of VEGFR and PDGFR families achieves greater antitumor activities than inhibition of either alone [3].

Despite recent advances in cancer treatment, the overall prognosis for malignant glioma patients remains poor. One of the hallmarks of malignant brain tumors is vigorous angiogenesis [13]. Recent approval of an anti-VEGF antibody, Avastin, for the treatment of malignant brain tumors shed some light on antiangiogenic approach for brain cancer therapy. Elevated VEGF and PDGF levels are commonly found in almost all types of brain cancers [7, 15], which may allow for unique treatment opportunities for multi-targeted tyrosine kinase inhibitors (TKIs) that target both VEGF/VEGFR and PDGF/PDGFR pathways. Linifanib (ABT-869) is a novel, orally active small molecule TKI that simultaneously inhibits VEGFR and PDGFR family members with minimal activity against unrelated receptor tyrosine kinases (RTKs). The compound has demonstrated potent antitumor efficacy in a broad range of preclinical cancer models, including hepatocellular carcinoma (HCC), non-small-cell lung carcinoma (NSCLC), renal cell carcinoma (RCC), colon carcinoma (CRC), breast carcinoma, and acute myeloid leukemia [1]. Its antiangiogenic property has been shown using growth factor-mediated angiogenesis model in rat cornea and uterine, but has not been tested in vivo in cancer models. To study the mechanistic relationship between antiangiogenesis and antitumor activities during linifanib treatment and to evaluate the effectiveness of linifanib against glioma, we characterized longitudinal functional and the accompanying structural changes in tumor blood vessels using DCE-MRI and IHC in an orthotopic 9L rat glioma model.

As increasing numbers of antiangiogenic agents progress through preclinical and clinical development, biomakers that can reliably assess vascular changes are important for monitoring antiangiogenic activities. DCE-MRI is a non-invasive imaging technique that is sensitive to MV function [8, 16], thus considered a promising pharmacodynamic (PD) marker for proof of concept and a biomarker for predicting and/or assessing treatment outcome. In the last 10 years, the method has been widely adopted in preclinical and clinical studies for the assessment of antiangiogenic treatment response [4, 8, 16]. Since there is no gold standard available to directly verify the PD parameters measured by DCE-MRI, the prognostic value of DCE-MRI is often tested against the treatment outcome. In this study, we examined correlations between early DCE-MRI measurements via K^{trans} and tumor inhibition to explore the prognostic value of DCE-MRI for linifanib treatment.

Methods

Experimental protocols for all studies were approved and closely monitored by the Abbott Institutional Animal Care and Use Committee, adhering to National Institutes of Health Guide for Care and Use of Laboratory Animals guidelines in facilities accredited by the Association for the Assessment and Accreditation of Laboratory Animal Care.

All MRI experiments were conducted on a 4.7-T/40 cm magnet (Varian Inc., Palo Alto, CA) with a 12-cm bore gradient insert operated via an INOVA imaging console (Varian Inc., Palo Alto, CA).

Tumor inoculation

Female Fischer 344 rats (150–170 g) were anesthetized with ketamine (80–100 mg/kg, i.p.) and xylazine (8–10 mg/kg, i.p.). During anesthesia, 9L glioma cells (5×10^5) suspended in 0.01 ml PBS were injected 3 mm in depth, measured from the surface of the skull, into the right striatum. Intracranial gliomas were established within 8 days following inoculation and reached an average size of 50–70 mm^3 by day 9–13, when DCE-MRI began.

Experimental design and treatment protocols

Three studies were conducted: examination of treatment efficacy in established rat orthotopic glioma model, evaluation of the time course of functional and structural changes in tumor blood vessels in response to the treatment of linifanib, measurements of the dose dependency of DCE-MRI measured vascular changes and assessment of the predictive value of early DCE-MRI measurements for linifanib-induced tumor growth inhibition.

Study I. Efficacy study

A total of 33 rats were inoculated with 9L glioma cells. Tumor growth was monitored using anatomical MRI every 3–6 days longitudinally throughout the study. Thirteen days after tumor induction, animals were size matched into two treatment groups receiving either vehicle (2% EtOH + 5% tween + 20% PEG 400 + 73% HPMC, $N = 16$) or linifanib (10 mg/kg in vehicle, $N = 17$) treatment. Vehicle or linifanib treatment was administered

orally twice daily (morning dose during 7–9 am and afternoon dose during 3–5 pm) until the end of the study (26 days after inoculation). Animals were observed closely for clinical signs of illness and humanely euthanized if animals lost >17% in weight or presented symptom/s such as ataxia, neuro-disorders, etc. according to IACUC guidelines.

Study II. Time course study

Thirteen days after cell inoculation, 26 animals were size matched into two groups to receive either vehicle (same as above) or linifanib (10 mg/kg) treatment using the same dosing paradigm as above. DCE-MRI was performed 1 day before the start of the treatment, the day treatment was started, and at days 1, 4, and 7 after treatment commenced. On each post-treatment imaging day, DCE-MRI was performed 2 h after the morning dose. Tumor-bearing brain tissues ($N = 3$ per group) were collected after DCE-MRI imaging for IHC assessment on days 1, 4, and 7 post-treatment.

Study III. Dose dependency study

Nine days after tumor inoculation, animals were size matched into four treatment groups: vehicle (same as above), linifanib at 1.5, 5, or 10 mg/kg, orally twice daily ($N = 6$ per group). Treatment (linifanib or vehicle) was continued for 10 days until the end of the study. DCE-MRI was performed 1 day before and 1 day after the start of the treatment. At day 1 after treatment starts, DCE-MRI was performed at 2 h after the morning dose. Tumor volume was measured longitudinally using MRI throughout the study.

MRI tumor volume measurement

Prior to MRI, rats were anesthetized using the same method described in tumor inoculation. A 4-cm volume coil (Morris Instrument Inc., Ottawa, Canada) was used for all MRI experiments. After sagittal scout imaging, ten 1.5-mm-thick transverse slices (with no gap in between) were prescribed to cover the entire glioma. A T_2-weighted imaging was performed using a spin echo sequence (TR = 1.5 s, TE = 0.8 s) with a field of view of 4 cm × 4 cm, a matrix of 256 × 128, and 2 repetitions. The total MRI time is approximately 10 min for each animal. Intracranial tumor area visualized based on T_2-weighted contrast in each slice was manually outlined using custom built software. The tumor volume from each slice was calculated from the product of the tumor area and the slice thickness. Three-dimensional tumor volumes (mm^3) were obtained by summing the tumor volumes from all tumor-containing slices.

DCE-MRI

Under anesthesia (the same used for inoculation), a rat tail vein was catheterized using a 25-G butterfly catheter pre-loaded with Gd-DTPA. The rat head was positioned in the same coil (used for tumor volume measurement) using an in-house built rat head holder with a tooth bite bar. Body temperature was maintained at 37°C during imaging using a heating blanket. A T_2-weighted anatomical MRI image (refer to tumor volume measurement section for imaging parameters) was acquired for tumor volume measurement and slice prescription for subsequent DCE-MRI. Four 1.5-mm-thick transverse brain slices containing glioma were identified. A pre-contrast T_1 map from the four chosen slices was measured and used for deriving dynamic changes in Gd concentration from imaging signal intensity. DCE-MRI was acquired using a T_1-weighted gradient echo sequence with imaging parameters of TR/TE = 150 ms/3 ms, a field of view of 3.0 × 3.0 cm^2, and an imaging matrix 256 × 128. Imaging time resolution is 19.2 s. After 10 baseline images, a bolus injection of Gd-DTPA (0.2 mmol/kg, iv) (Bayer HealthCare Pharmaceuticals, Wayne, NJ, USA) was administered via tail vein, imaging acquisition was continued for 8 more minutes after contrast agent injection.

DCE-MRI imaging analysis

All calculations were performed using custom built software developed in Interactive Data Language (IDL) (ITT Visual Information Solutions, Boulder, CO). DCE-MRI data were analyzed based on the two-compartment tracer kinetic modeling described by Tofts et al. [22]. First, the recorded time course DCE-MRI signal was converted into time course contrast agent concentration with the aid of pre-contrast T_1 measurement. The plasma contrast agent concentration was derived from the arterial input function measured from large vessels present in the imaging slices. The Tofts-Kermode equations [22] associating tissue and plasma contrast agent concentrations were solved via curve fitting to calculate pharmacokinetic parameter K^{trans}, the volume transfer constant from blood pool to extravascular extracellular space per unit tissue volume. The calculation was carried out pixel-by-pixel from manually outlined tumor regions of all prescribed slices. Because of the heterogenous nature of tumor tissue, a log transform was applied to pixel-wised K^{trans} data to achieve normal distribution, and thereafter, their geometric means were calculated to provide an average K^{trans} for each lesion.

Tumor tissue collection and preparation for blood vessel assessment

In study II after completion of the DCE-MRI experiments, three tumor-bearing brains (per time point, per treatment group) were collected from rats receiving 1, 4, or 7 days of linifanib or vehicle. Individual tumor vessels were assessed by tail vein injection of 200 μg of fluorescein isothiocyanate-labeled Lycopersicon esculentum (tomato) lectin (lectin/FITC, Vector Laboratory, CA) immediately after DCE-MRI. The lectin/FITC was allowed to circulate 10–15 min before tumor tissue collection. The brain was detached from skull and immersed in ethanol with dry ice for 1 min and then transferred into liquid nitrogen. The frozen tumor-bearing brain was cut into coronal sections of 50 μm for the assessment of global vasculature. Sections of 20 μm were cut and fixed with 4% paraformaldehyde for 60 min, then washed with PBS and air dried. The slides were stored at 4°C for further IHC staining.

Immunohistochemistry

Two micrograms of each primary antibody was used to stain the receptors and basement membrane collagen IV in tumor tissues: (a) phospho-VEGFR-2 antibody (Tyr1214, Spring Bioscience, Pleasanton, CA), (b) phospho-PDGFR-β (Tyr1009, Santa Cruz Biotechnology, Santa Cruz, CA), and (c) anti-collagen IV (Abcam Inc., Cambridge, MA). The specificity of the antibody signal was determined by use of matched isotype control antibodies as well as blocking the binding of the phosphorylated VEGFR-2 (p VEGFR-2) and PDGDR-β (pPDGDR-β) antibodies by pre-incubation with the synthetic peptides used to generate the antibodies (data not shown), synthetic PDGFR-β peptide (Tyr1009, Santa Cruz Biotechnology, Santa Cruz, CA) and synthetic VEGFR-2 peptide (Tyr1214, Genemed Synthesis, San Antonio, TX).

IHC was performed for identification of pVEGFR-2 and pPDGFR-β expression on tumor tissues. First, the tumor tissue sections were permeablized with 0.3% triton x-100 in phosphate-buffered saline (PBS) and incubated with either primary antibody for 2 h at room temperature. Subsequently, a specific polymer system followed by horseradish peroxidase (HRP) and 3, 3′ diaminobenzidine (DAB) was used for immunostaining detection (Biocare Medical, Concord, CA). Finally, the tissue sections were counterstained with hematoxylin. For collagen IV dual labeling on lectin/FITC-infused tissues, collagen IV antibody was conjugated with Alexa 594 (Zenon labeling technology, Invitrogen, Carlsbad, CA) then incubated with the slides overnight at room temperature. Stained slides were washed with PBS and rinsed with distilled H_2O and covered with prolong anti-fade mounting medium containing DAPI (4′, 6-diamidino-2-phenylindole, Invitrogen, Carlsbad, CA). Fluorescent images or chromogenic images were captured with Zeiss AxioPhot 2 fluorescent microscope (Carl Zeiss, Germany).

Histological image acquisition and analysis

Tumor sections were visualized using either bright or fluorescence filters: DAPI for nuclei, FITC or Alexa 594 for lectin and collagen IV, and chromogenic detection for receptor staining. Images were captured with a Zeiss Axiocam camera connected to the microscope using AxioVision 4.6 software. In general, 2–4 sections in each of 3 tumors from each treatment group were examined, and 4–6 highly vascularized areas (0.4 mm^2/each) from each section were randomly selected for image acquisition and analysis. MV were identified by fluorescence-labeled lectin vascular infusion [14], and MV densities are quantified at $\times$200 magnification. Disruptive basement membrane coverage was defined as a MV surrounded by discontinuous collagen IV-positive staining. The proportion of disruptive basement membrane MV was calculated by the ratio of the number of disruptive basement membrane MV to the total number of MV in the same area.

Pathological scores were determined for pPDGFR-β and pVEGFR-2 immunostaining. The stain intensity for each antibody was assessed using the scale of 0–3 (0 = no staining; 1 = weak staining; 2 = medium staining; and 3 = strong staining. The scores were divided into 2 groups (0–1) and (2–3) prior to statistical analysis. Isotype antibody and peptide competitive staining were used as negative controls for each antibody.

Statistical analysis

All statistical analyses were performed using SAS or JMP (SAS Institute, Cary, NC) unless stated otherwise. For comparison, ANOVA and Tukey-HSD tests or two-sample t test were applied to compare the average K^{trans} from different treatment groups. A mixed-effect model was fitted to estimate the MV diameter and density for each group. The two-sample t-test was applied to identify differences between the treatment groups in MV diameter, density, or the basement membrane coverage per section. For IHC staining intensity assessment, Wilcoxon test was used for the number of tumors with the scale $\geq$2 or $<$2. Values are expressed as mean ± SE. Statistical analysis was carried out using the JMP 8.0 software. P value $<$0.05 was considered a statistically significant difference.

Spearman rank based correlation analysis was done to evaluate the linear relationship of the baseline K^{trans}, percent change in K^{trans} (1 day post treatment vs 1 day before treatment) with tumor volume changes following treatment

for 7 days for all treatment groups. Receiver operating characteristic (ROC) analysis was done to assess the baseline K^{trans} and the percent K^{trans} changes at 1 day after relative to 1 day before treatment as predictors of response in tumor growth. A fully embedded fivefold cross validation of the ROC was also performed to assess the variability of the whole procedure in terms of sensitivity and specificity. Statistical analysis of the assessment of whether K^{trans} was a good predictor of tumor inhibition was done using R (R Development Core Team, Vienna, Austria).

Results

Linifanib treatment inhibited tumor growth

Dose-dependent antitumor activity of linifanib has been shown in our previous efficacy study in the 9L rat glioma model when treatment began before tumors were established [1]. The current study was designed to test tumor inhibition by linifanib (10 mg/kg, po, bid) against established gliomas. Treatment began 13 days after tumor inoculation when average tumor volume was $\sim$70 mm^3. No tumor volume changes were observed 1 day after the treatment. Tumor volume measurement after 7 days of treatment showed a significant tumor volume reduction in the linifanib-treated group compared with the vehicle-treated group (Fig. 1). The average tumor volume of linifanib-treated group was 66 $\pm$ 7 mm^3 on day 7 after the treatment. Compared to the vehicle-treated tumors, which had an average tumor volume of 149 $\pm$ 30 mm^3, linifanib treatment produced a 58% reduction in tumor growth ($P < 0.01$). Linifanib treatment dosed orally at 10 mg/kg twice daily was well tolerated. No significant weight loss was observed from linifanib-treated animals. The average body weight was 171 $\pm$ 2 and 170 $\pm$ 5 g for linifanib and vehicle-treated groups, respectively, after 7 days of treatment.

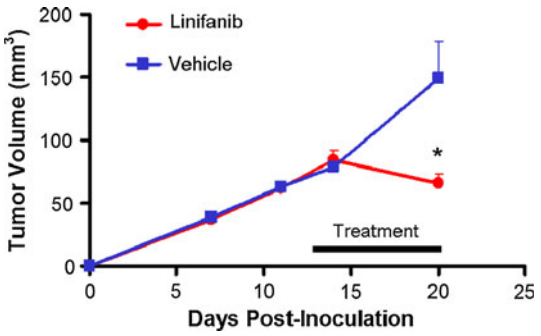

Fig. 1 Antitumor efficacy of linifanib (10 mg/kg, bid, po) against established 9L rat gliomas. (*$P < 0.01$) *Error bars* shown are SE

Linifanib reduces tumor K^{trans}

Representative DCE-MRI images acquired illustrating the signal enhancement observed at 8 min after Gd-DTPA contrast agent injection are shown in Fig. 2a. No signal enhancement was detected in normal brain, but significant signal enhancement was observed in tumors. Comparing the images measured at 2 h, 1 and 4 days after beginning treatment with those measured before treatment, signal enhancement in the vehicle-treated tumors was very similar at all time points. In contrast, the linifanib-treated tumors showed a decrease in signal enhancement at 2 h after the treatment and a greater reduction was observed at later time points.

Gross evaluation of K^{trans} values within gliomas indicated that tumor K^{trans} distribution is highly heterogeneous. In most cases, higher K^{trans} values were found to be in the tumor margin, while lower K^{trans} values were found in the center of the tumor. The mean tumor K^{trans} values measured prior to treatment were not different between the vehicle- and linifanib-treated group. A significant reduction (by 37 $\pm$ 13%, $P < 0.05$) in the mean tumor K^{trans} was observed at 2 h after linifanib treatment compared with the vehicle-treated group. More substantial decreases in tumor K^{trans} were observed at day 1 after treatment (decreased by 72 $\pm$ 15%, $P < 0.01$ vs. vehicle) and remained at a similar level at day 4 (decreased by 72 $\pm$ 9%, $P < 0.01$ vs. vehicle) and day 7 after treatment (decreased by 75 $\pm$ 32%, $P < 0.05$ vs. vehicle; see Fig. 2b). In contrast, K^{trans} in vehicle-treated rats did not change significantly over time ($P > 0.05$) as seen in Fig. 2b. To verify that the decrease in tumor K^{trans} was pharmacologically correlated with linifanib treatment, we evaluated tumor K^{trans} responses to linifanib at multiple doses. Compared with the vehicle-treated group, K^{trans} measured at day 1 after treatment was decreased by 40 $\pm$ 39% ($P = 0.67$), 80 $\pm$ 21% ($P < 0.05$), and 79 $\pm$ 20% ($P < 0.05$) in the 1.5, 5.0, and 10 mg/kg groups, respectively (Fig. 2c).

Prediction of tumor growth inhibition using K^{trans}

As described above, the tumor K^{trans} changed rapidly after linifanib treatment. Significant reduction in K^{trans} was observed at 2 h and 1 day after linifanib treatment when no significant tumor volume reduction could be detected. We examined the association of the baseline K^{trans} measured 1 day prior to the beginning of treatment and percent changes in K^{trans} measured 1 day after the beginning of treatment with the percent changes in tumor volume at 7 days after the treatment. There is a positive correlation between the baseline K^{trans} with tumor growth; the Spearman's rank correlation was 0.59 ($N = 36$, $P = 0.0003$, Fig. 3a). Receiver operating characteristics (ROC) analysis indicated that using baseline K^{trans} as a predictive biomarker for tumor growth in

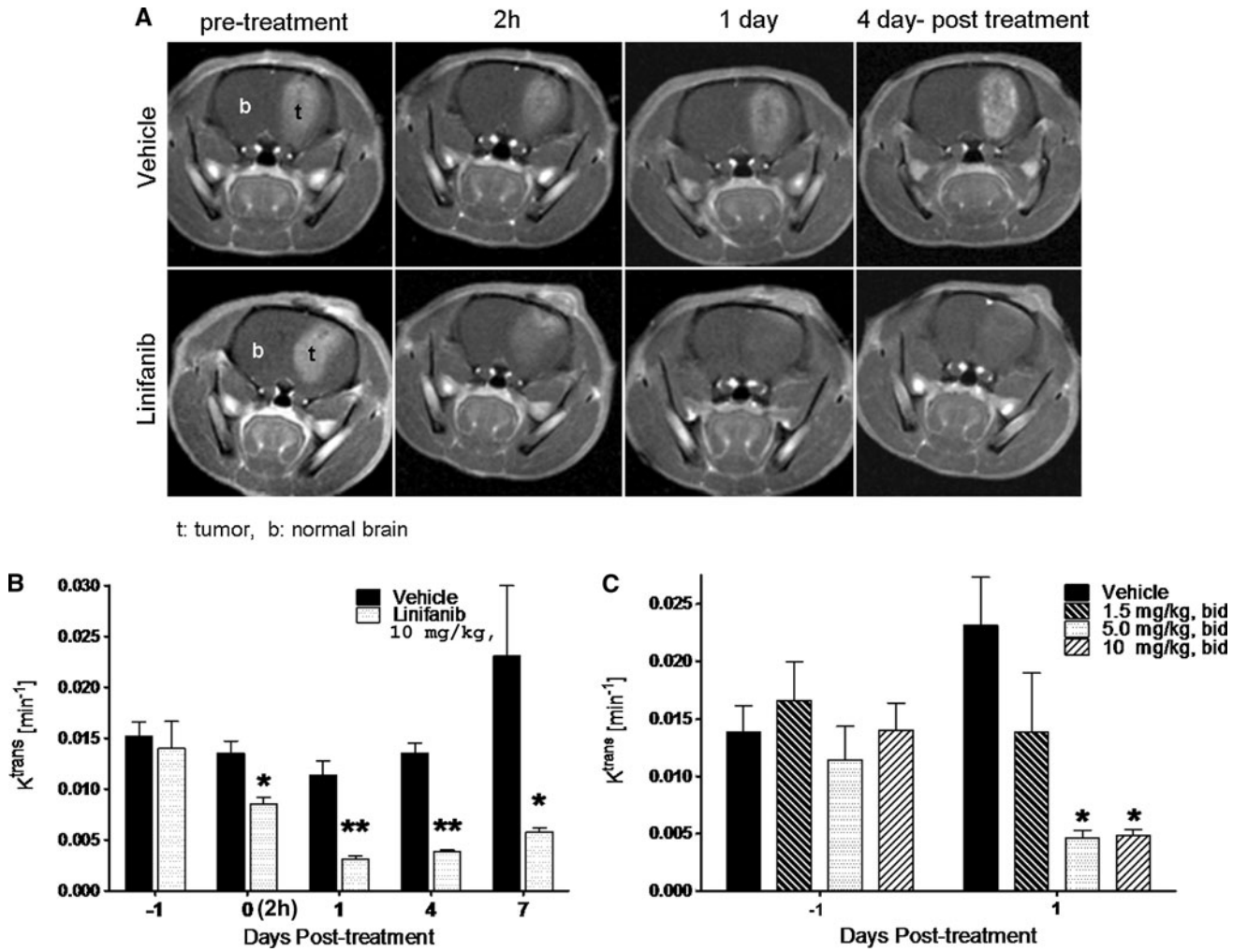

Fig. 2 **a** Longitudinal DCE-MRIs showing contrast enhancement in rat glioma 8 min after Gd-DTPA injection. In a vehicle-treated rat, significant contrast enhancement was evident within tumor regions, and the signal enhancement level was similar across all time points. In contrast, in a rat treated with linifanib, contrast enhancement within tumor decreased. The reduction in contrast enhancement was more pronounce 1 and 4 days after linifanib treatment compared to 2 h post-treatment. **b** Longitudinal changes in K^{trans} ($N = 4$–6 per group) in response to the linifanib treatment (10 mg/kg, bid, po). K^{trans} decreased immediately following the first dose of linifanib (day 0) and more pronounced reduction was observed after 1, 4, and 7 days after treatment comparing to either baseline (day −1) or vehicle-treated group. **c** The linifanib treatment-induced decreases in K^{trans} ($N = 7$–10 per group) measured 1 day after linifanib treatment were dose dependent. $^*P < 0.05$, $^{**}P < 0.01$ compared to the vehicle-treated group. *Error bars* shown are SE

this study was 76% accurate with a specificity of 83% (Fig. 3c). The optimal cutoff of baseline K^{trans} for tumor response was 0.0131 (min^{-1}). Although significant changes in K^{trans} were only observed in linifanib-treated animals and were dose dependent reflecting the pharmacological activities induced by linifanib, the percent K^{trans} changes were not as good of a predictor for tumor growth inhibition compared to baseline K^{trans} with a Spearman's rank correlation of 0.25 ($N = 27$, $P = 0.18$, Fig. 3b).

Tumor vasculature by IHC

9L glioma cancer cells inoculated in rat brain produced a syngeneic orthotopic glioma model. These tumors grew rapidly, and the tumor margins were well delineated with little infiltration into the contiguous normal brain (Fig. 4a). Fluorescence-labeled lectin injected into bloodstream binds rapidly and uniformly to the luminal surface of vasculature, allowing visualization of actively perfused blood vessels [6]. In vehicle-treated gliomas, blood vessel networks were chaotic and most of the blood vessels were dilated and leaky, evidenced by an increased vessel diameter and diffused lectin outside of the vessel lumen. Fewer intact blood vessels were present within gliomas than in the normal brain where blood vessels were well structured and organized. Tumor blood vessels along the tumor border intersected with normal blood vessels, indicating co-option of normal vessels to supply blood to the tumor (Fig. 4b, c).

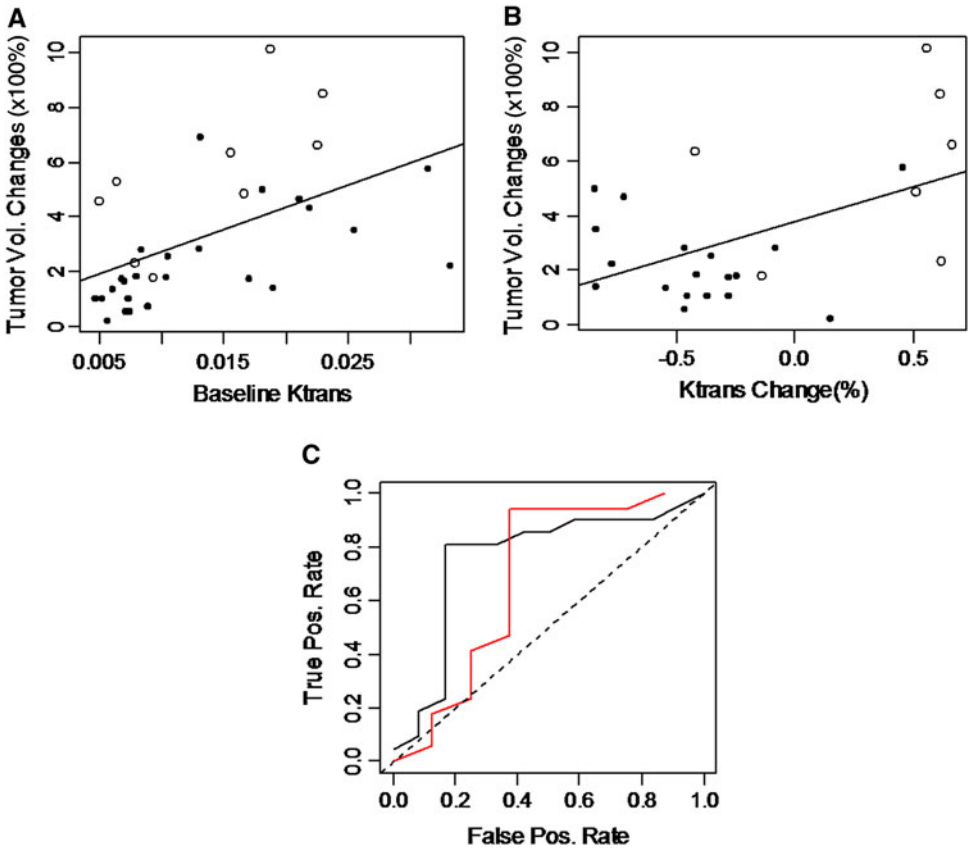

Fig. 3 **a** Positive correlation between baseline tumor K^{trans} measured 1 day prior to treatment and tumor growth measured at 7 days after treatment ($N = 36$, $P = 0.0003$). **b** Positive correlation between percent tumor K^{trans} changes (1 day after relative to 1 day before the treatment) and tumor growth inhibition measured at 7 days after treatment ($N = 27$, $P < 0.1802$). *Open circle*—vehicle-treated animals, *solid circle*—linifanib-treated animals. **c** ROC analysis for the predictive power of using the baseline K^{trans} to predict tumor response shows the prediction is 76% accurate and 83% specific

Linifanib treatment inhibited phosphorylation of PDGF-β and VEGFR-2

IHC staining of glioma samples confirmed in vivo inhibition of the target receptors pPDGFR-β and pVEGFR-2 by linifanib at all time points. The binding of antibodies specific for the phosphorylated receptors was measured semi-quatitatively using the traditional 0–3 scale. We found that pVEGFR-2 was predominately located in endothelial cells and tumor cells, while pPDGFR-β was predominately located in tumor cells. Untreated baseline lesions had high expression levels of both phosphorylated receptors with a median staining intensity of 3+. Following treatment with linifanib, the mean staining intensity of pPDGFR-β on 1, 4 and 7 days were 0.75, 0.67 and 0.67, while vehicle values were 3 at all time points ($P = 0.02$, 0.03 and 0.03, respectively). Similarly, following treatment with linifanib, the mean staining intensity of pVEGFR-2 on 1, 4, and 7 days were 0.75, 0.67, and 0.67, while vehicle values were 3, 2.67, and 3 ($P = 0.03$, 0.04, and 0.03, respectively). The elimination of stain intensity of the receptors by linifanib at all time points was evident (Fig. 5), which confirmed the inhibition of the target receptors by linifanib.

Linifanib treatment reduced MV diameter and density and improved vascular wall integrity

In vehicle-treated gliomas, peri-vascular tumor cells stained with lectin/FITC indicated the presence of vessel dilation and leakage (Fig. 6a). Following linifanib treatment, blood vessels that remained intact within tumors appeared to be straight and less leaky with improved vascular wall integrity, which was morphologically similar to normal vessels (Fig. 6b, c). A set of vascular parameters including vessel density, diameter and basement membrane coverage (Mean ± SE) were assessed to investigate the impact of linifanib treatment on the tumor vasculature. MV density was significantly reduced following linifanib treatment when compared to baseline (20.0 ± 3.09 MV per 0.4 mm^2 area) and vehicle-treated group on day 4 (10.0 ± 4.7 vs. 22 ± 3.63 vehicle, MV per 0.4 mm^2 area, $P < 0.01$) and day 7 (8.5 ± 2.68 vs. 18 ± 2.6 vehicle, MV per 0.4 mm^2 area, $P < 0.01$) as seen in Fig. 6e. MV diameter significantly decreased only at 7 days after treatment with linifanib (8.0 ± 1.18 μm vs. 13.0 ± 1.19 μm vehicle, $P < 0.01$) as seen in Fig. 6d. In this study, we used collagen IV, a main structural component of the basement membrane, to assess linifanib effect on the

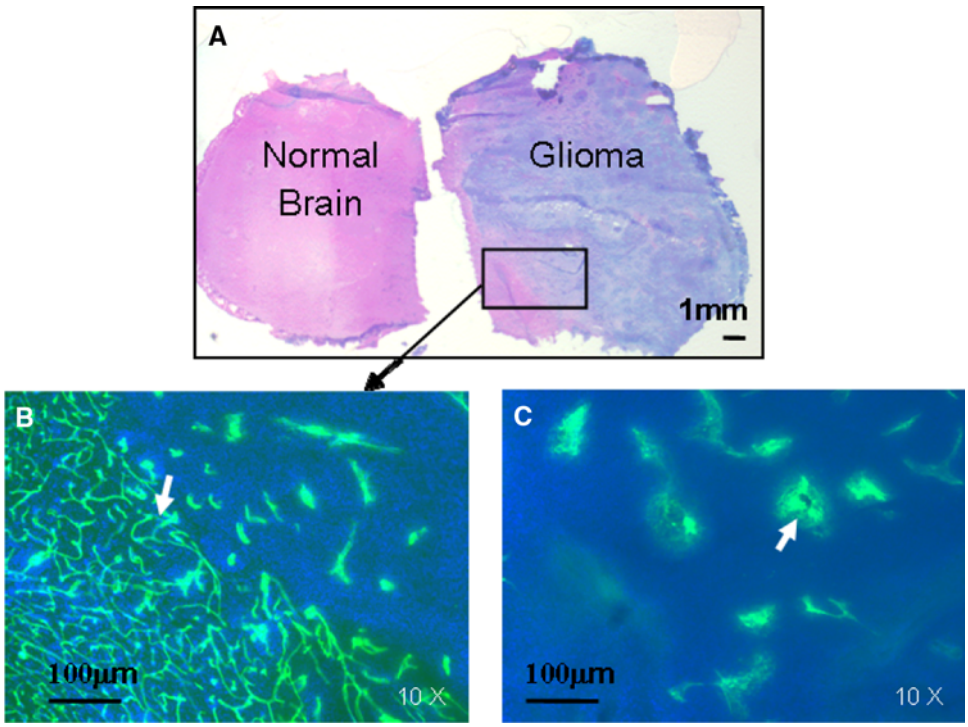

Fig. 4 **a** Global vasculature in a 9L glioma-bearing rat brain. H&E staining presents general morphology of a vehicle-treated rat brain with a xenograft 9L glioma. **b** Lectin/FITC vessel (*green*) labeling presents a well-organized blood vessel network composed of well-structured individual vessels in normal brain. *Arrow* head points to tumor edge, where ill-formed blood vessels co-op with normal blood vessels. **c** chaotic, dilated vessels in glioma. *Arrow* head points dilated vessel lumen and extravasation of lectin/FITC dye. *Bars* present 1 mm in **a**, and 100 μm in **b** and **c**

vascular wall integrity. The basement membrane coverage was disrupted in vehicle control tumor vessels. Following linifanib treatment at days 4 and 7, the basement membrane coverage was continuous and tightly associated with the vessels. The improvement of vascular wall integrity was indicated by reduction in percent disruptive basement membrane, which was significantly reduced following treatment with linifanib when compared with baseline (70 ± 8% per tumor) and vehicle control on day 4 (13 ± 4% vs. 81 ± 9% vehicle, $P < 0.01$) and day 7 (16 ± 4% vs. 91 ± 6% vehicle, $P < 0.01$) (Fig. 6f). No significant changes in MV density, diameter and basement membrane at day 1 after the treatment from baseline (Fig. 6).

Discussion

Linifanib is a novel ATP-competitive inhibitor with potent activity toward VEGF and PDGF RTKs. We have previously shown that linifanib exhibits antitumor activities across a wide range of tumor models [1]. In the 9L rat glioma model, linifanib inhibited tumor growth when applied 2 days after tumor inoculation (before the solid tumors have formed) in a dose-dependent manner. Our current study demonstrated that linifanib is also effective in inhibiting tumor growth of established vascularized gliomas. Concurrent tumor vascular changes in response to linifanib treatment were also studied. Linifanib treatment induced a rapid dose-dependent reduction in tumor vessel permeability as measured by K^{trans} and at a later time point induced significant structural changes in the remaining tumor microvessels. The DCE-MRI-derived tumor vessel permeability K^{trans} measured before treatment showed a positive correlation with tumor growth. The correlation between the early reductions in K^{trans} with tumor growth inhibition was also positive, but not statistically significant.

Tumor angiogenesis is organ specific and involves complex tumor-host interactions [13]. To optimally imitate angiogenesis in a model that closely mimics an endogenous tumor, we chose an orthotopically implanted rat syngeneic 9L glioma model to evaluate the antiangiogenic effects of linifanib. The 9L glioma model, a rat gliomsarcoma model, possesses many relevant features of human gliomas [21]. The expression pattern of VEGF and PDGF and the autocrine/paracrine regulations via VEGF/VEGFRs and PDGF/PDGFRs in 9L glioma are well documented and showed a close similarity to those in human gliomas [18]. We observed ill structured MV in 9L glioma that are disorganized, dilated, leaky, and lack the normal blood–brain barrier function, which is in agreement with previously published reports and is consistent with reported human glioma MV [19, 23].

VEGF signaling through VEGFR-2 in endothelial cells is a major component of tumor angiogenesis and a target of linifanib [10]. Antiangiogenic treatment targeting VEGF/VEGFR signaling has proven to be an effective approach for cancer treatment. Our results demonstrate a significant tumor growth inhibition from linifinib at a dose producing concomitant inhibition of VEGFR-2 and PDGFR-β in rat

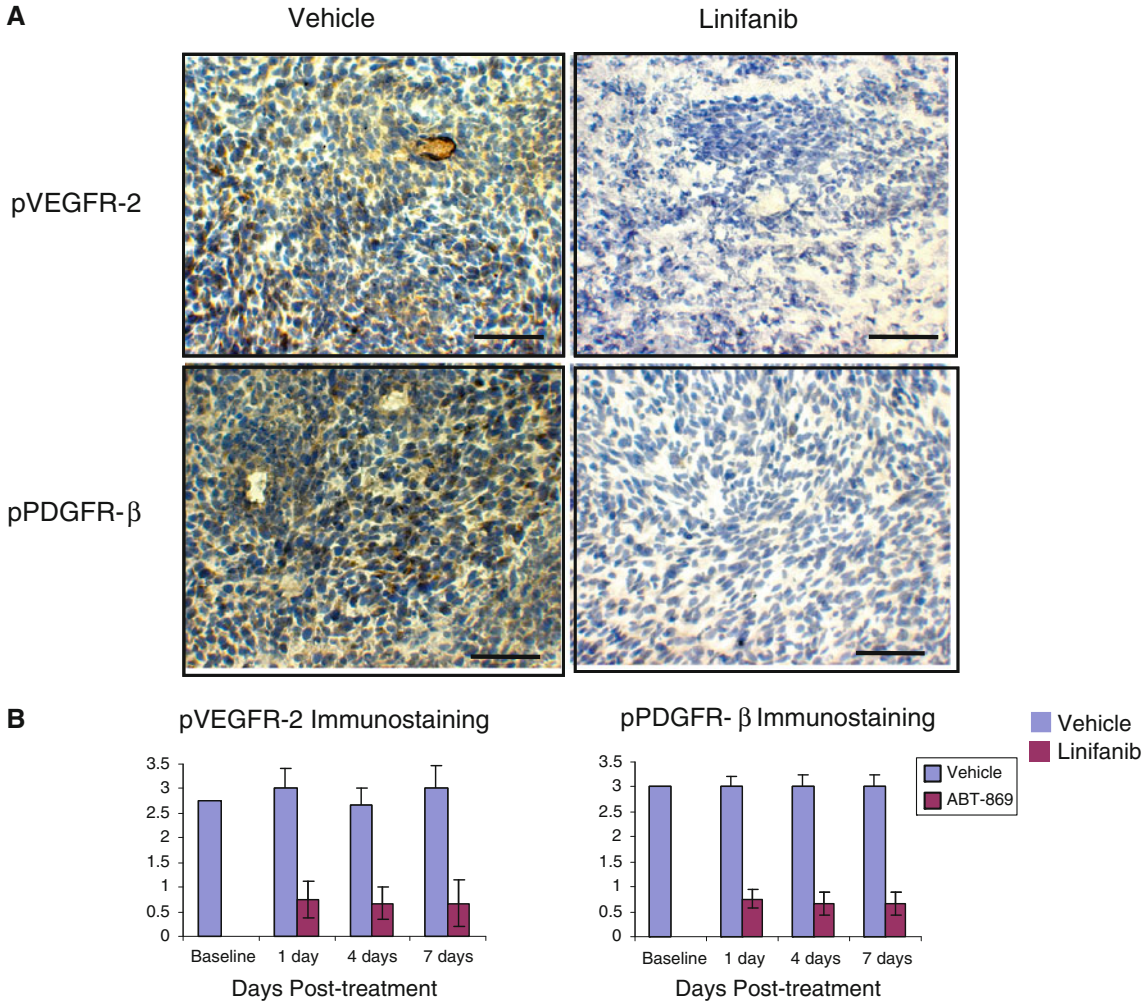

Fig. 5 **a** Linifanib inhibited phosphorylation of VEGFR-2 and PDGFR-β. The receptor phosphorylation was detected using immunostaining of pVEGFR-2 and pPDGFR-β antibodies (HRP/DAB detection). The inhibition of receptor phosphorylation was indicated by a decrease in the brown stain intensity. **b** Quantification of stain intensity on the baseline, 1, 4, and 7 days treatment with or without linifanib (details see "Methods"). *Bars* present 100 μm

gliomas. The antiangiogenic properties observed in this study with linifanib treatment such as decreasing vessel leakiness, inhibiting neo-vessel growth, and vessel dilation are consistent with the vascular consequences of VEGF-2 inhibition generated by the established antiangiogenic drug Avastin. The reduced vessel permeability and dilation with treatment help decrease interstitial fluid pressure and consequently alleviate edema, which is a significant benefit for glioma patients [11]. Therefore, antiangiogenesis therapy via VEGFR-2 inhibition is likely responsible, at least in part, for the antitumor efficacy of linifanib. However, Avastin failed to inhibit intracranial tumor growth [5], whereas linifanib produced significant single-agent tumor growth inhibition in both early- and late-stage gliomas. In addition, MV density measured after treatment with linifanib was significantly lower than the baseline level, indicating that linifanib not only prunes neovessels but also targets existing tumor vasculature. These observations suggest that additional mechanisms are involved and contribute to the antitumor efficacy of linifanib.

Linifanib also targets PDGF, a growth factor involved in many cancers, in addition to VEGF. A large body of evidence suggests that PDGF plays an important role in regulating glioma angiogenesis and growth [15]. PDGF is a mitogen for glioma cell proliferation and is found to upregulate VEGF expression. Although linifanib is not a general antiproliferative agent, it can impose antitumor effects via inhibition of PDGF-mediated cell proliferation and produces more efficient antiangiogenesis when synergizing VEGF inhibition via PDGF inhibition. In our study, the tumor blood vessels in established 9L gliomas lacked pericyte coverage and the basement membrane was only loosely associated with endothelial cells. Such disrupted vasculature sensitized the vascular endothelial cells for

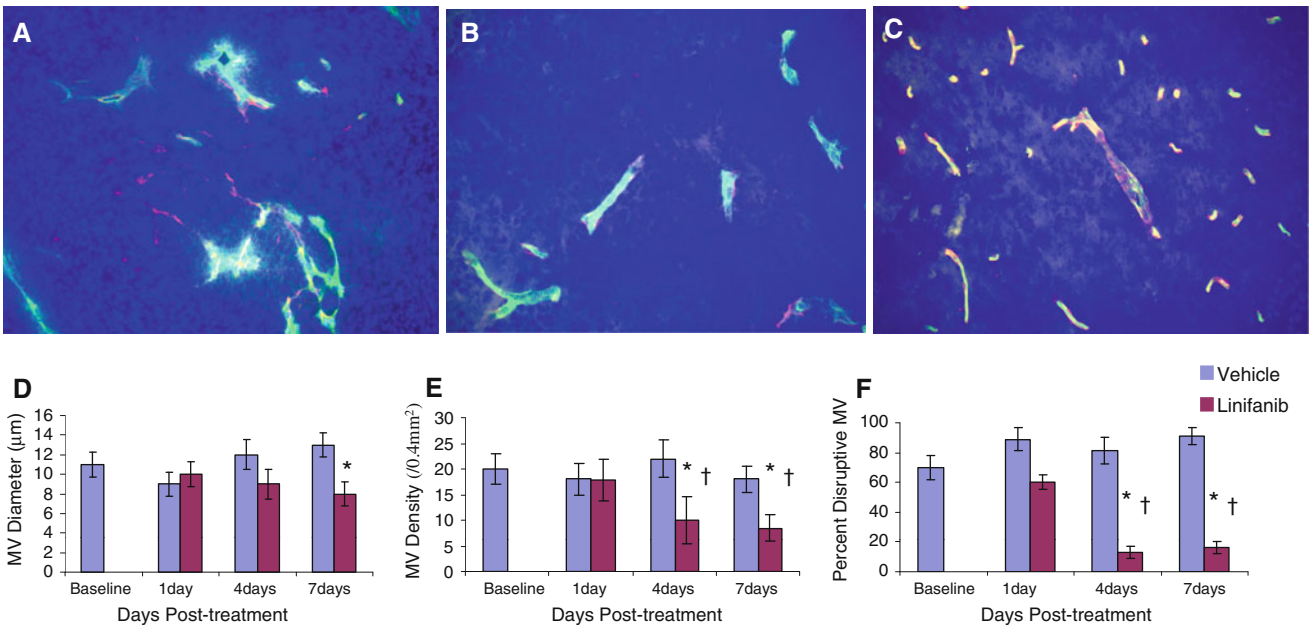

Fig. 6 Linifanib effects on the tumor vasculature. Lectin/FITC (*green*) infusion-labeled vessels and collagen IV/Alexa 594 (*red*)-labeled basement membrane. DAPI (*blue*)-stained nuclei. Vessels with disruptive basement membrane coverage in a vehicle-treated glioma were leaky indicated by lectin/FITC staining of peri-tumor vessel cells. **a** Basement membrane coverage of tumor MV was improved after linifanib treatment for 4 days. **b** Vessels in normal rat brain had complete basement membrane coverage. **c** Quantification of MV diameter **d**, MV density **e**, and percent disruptive basement membrane **f** with or without linifanib treatment. $*P < 0.01$ compared to vehicle, $\dagger P < 0.01$ compared to the baseline. *Bars* present 100 μm. *Error bars* shown are SE

apoptosis under VEGF deprivation [2]. This may explain the antivascular effects of linifanib on the existing tumor vasculature. In evaluating antitumor efficacy of different TKIs, Bergers and collaborators found that inhibition of PDGFR-β is required for reducing tumor growth in late-stage tumors where inhibition of VEGF signaling alone was not effective. Our results showed efficacy of linifanib inhibiting both early- and late-stage tumor growth, thus demonstrating the enhanced antitumor benefits against gliomas when simultaneously inhibiting both VEGF and PDGF pathways.

Linifanib treatment led to a significant phenotype change in tumor blood vessels characterized by decreased vessel permeability, dilation, vessel density, and better vessel wall integrity in the remaining vessels. These properties are consistent with the proposition of vascular normalization and can exert significant impact on oxygen and drug delivery. While improved vessel integrity and a better organized vessel network can enhance oxygen and drug delivery, the decreased vessel permeability and density pose the opposite effects. The net outcome is determined by the ending balance between vessel pruning and the functional improvement of normalized vessel structure under a specific treatment schedule. Decreased Gd-DTPA uptake in tumors receiving linifanib suggests hindrance to drug delivery due to the reduced tumor vessel leakiness and/or restoration of the BBB. Such an effect occurs immediately following the treatment and persists as treatment continues. The degree of reduction is sensitive to the dose level of linifanib. Significant structural normalization comes after chronic dosing and remained stable as treatment continued. The overall consequence of linifanib on drug delivery when used in combination therapy requires further studies and is currently under evaluation in our laboratory.

To assess the treatment effects of linifanib non-invasively, DCE-MRI was investigated as a possible tool with translational potential. Since there is no gold standard available to directly verify the PD parameters measured by DCE-MRI, the prognostic value of DCE-MRI is often tested against the treatment outcome by correlating the DCE-MRI derived parameters, among which K^{trans} is mostly studied, with clinical prognostic factors. In our study, we tested the correlation of baseline K^{trans} and early K^{trans} change with tumor growth inhibition and found that higher K^{trans} at baseline correlates with faster glioma growth. High baseline K^{trans} reflects high vessel permeability, which is often associated with high levels of VEGF in the tumor [10, 17]. In characterizing glioma progression, high levels of VEGF and high vessel permeability were found to be associated with a high grade of glioma [15], which may contribute to the positive correlation between baseline K^{trans} and tumor growth found in our study.

In conclusion, the results of this study show that linifanib produced in vivo antiangiogenic and antivascular

effects, and consistent single-agent activities against both early- and late-stage glioma growth via concomitant inhibition of VEGF-R and PDGF-R pathways. VEGF and PDGF are important growth factors regulating glioma progression; our study suggests potentially unique opportunity of linifanib in managing glioma patients. In addition, results from DCE-MRI measured K^{trans} show that K^{trans} is sensitive to linifanib-induced vascular changes and can therefore be a useful PD marker for proof-of-concept of compound action in clinical trials.

Acknowledgments The authors acknowledge Dr. Ke Zhang for his help with statistical analysis and Timothy Bowlin for his contribution to the experiments. The authors also wish to thank Drs. Jaymin Upadhyay, Feng Luo, Sarah Mudd, and Rikki Waterhouse for editing the manuscript and Prasant Chandran for help with preparation of the manuscript. All studies were supported by Abbott Laboratories research funding.

References

1. Albert DH, Tapang P, Magoc TJ, Pease LJ, Reuter DR, Wei RQ, Li J, Guo J, Bousquet PF, Ghoreishi-Haack NS, Wang B, Bukofzer GT, Wang YC, Stavropoulos JA, Hartandi K, Niquette AL, Soni N, Johnson EF, McCall JO, Bouska JJ, Luo Y, Donawho CK, Dai Y, Marcotte PA, Glaser KB, Michaelides MR, Davidsen SK (2006) Preclinical activity of ABT-869, a multitargeted receptor tyrosine kinase inhibitor. Mol Cancer Ther 5:995–1006
2. Bergers G, Benjamin LE (2003) Tumorigenesis and the angiogenic switch. Nat Rev Cancer 3:401–410
3. Bergers G, Song S, Meyer-Morse N, Bergsland E, Hanahan D (2003) Benefits of targeting both pericytes and endothelial cells in the tumor vasculature with kinase inhibitors. J Clin Invest 111:1287–1295
4. Checkley D, Tessier JJ, Kendrew J, Waterton JC, Wedge SR (2003) Use of dynamic contrast-enhanced MRI to evaluate acute treatment with ZD6474, a VEGF signalling inhibitor, in PC-3 prostate tumours. Br J Cancer 89:1889–1895
5. de Groot JF, Fuller G, Kumar AJ, Piao Y, Eterovic K, Ji Y, Conrad CA (2010) Tumor invasion after treatment of glioblastoma with bevacizumab: radiographic and pathologic correlation in humans and mice. Neuro Oncol 12:233–242
6. Debbage PL, Griebel J, Ried M, Gneiting T, DeVries A, Hutzler P (1998) Lectin intravital perfusion studies in tumor-bearing mice: micrometer-resolution, wide-area mapping of microvascular labeling, distinguishing efficiently and inefficiently perfused microregions in the tumor. J Histochem Cytochem 46:627–639
7. Dunn IF, Heese O, Black PM (2000) Growth factors in glioma angiogenesis: FGFs, PDGF, EGF, and TGFs. J Neurooncol 50:121–137
8. Evelhoch JL, LoRusso PM, He Z, DelProposto Z, Polin L, Corbett TH, Langmuir P, Wheeler C, Stone A, Leadbetter J, Ryan AJ, Blakey DC, Waterton JC (2004) Magnetic resonance imaging measurements of the response of murine and human tumors to the vascular-targeting agent ZD6126. Clin Cancer Res 10:3650–3657
9. Ferrara N, Hillan KJ, Gerber HP, Novotny W (2004) Discovery and development of bevacizumab, an anti-VEGF antibody for treating cancer. Nat Rev Drug Discov 3:391–400
10. Folkman J, Merler E, Abernathy C, Williams G (1971) Isolation of a tumor factor responsible for angiogenesis. J Exp Med 133:275–288
11. Friedman HS, Prados MD, Wen PY, Mikkelsen T, Schiff D, Abrey LE, Yung WK, Paleologos N, Nicholas MK, Jensen R, Vredenburgh J, Huang J, Zheng M, Cloughesy T (2009) Bevacizumab alone and in combination with irinotecan in recurrent glioblastoma. J Clin Oncol 27:4733–4740
12. Glade-Bender J, Kandel JJ, Yamashiro DJ (2003) VEGF blocking therapy in the treatment of cancer. Expert Opin Biol Ther 3:263–276
13. Jain RK, di Tomaso E, Duda DG, Loeffler JS, Sorensen AG, Batchelor TT (2007) Angiogenesis in brain tumours. Nat Rev Neurosci 8:610–622
14. Minamikawa T, Miyake T, Takamatsu T, Fujita S (1987) A new method of lectin histochemistry for the study of brain angiogenesis. Histochemistry 87:317–320
15. Nieder C, Schlegel J, Andratschke N, Thamm R, Grosu AL, Molls M (2003) The role of growth factors in central nervous system tumours. Anticancer Res 23:1681–1686
16. O'Connor JP, Jackson A, Parker GJ, Jayson GC (2007) DCE-MRI biomarkers in the clinical evaluation of antiangiogenic and vascular disrupting agents. Br J Cancer 96:189–195
17. Plate KH, Breier G, Weich HA, Risau W (1992) Vascular endothelial growth factor is a potential tumour angiogenesis factor in human gliomas in vivo. Nature 359:845–848
18. Plate KH, Mennel HD (1995) Vascular morphology and angiogenesis in glial tumors. Exp Toxicol Pathol 47:89–94
19. Plate KH, Risau W (1995) Angiogenesis in malignant gliomas. Glia 15:339–347
20. Richardson TP, Murphy WL, Mooney DJ (2001) Polymeric delivery of proteins and plasmid DNA for tissue engineering and gene therapy. Crit Rev Eukaryot Gene Expr 11:47–58
21. Sibenaller ZA, Etame AB, Ali MM, Barua M, Braun TA, Casavant TL, Ryken TC (2005) Genetic characterization of commonly used glioma cell lines in the rat animal model system. Neurosurg Focus 19:E1
22. Tofts PS (1997) Modeling tracer kinetics in dynamic Gd-DTPA MR imaging. J Magn Reson Imaging 7:91–101
23. Yuan F, Leunig M, Huang SK, Berk DA, Papahadjopoulos D, Jain RK (1994) Microvascular permeability and interstitial penetration of sterically stabilized (stealth) liposomes in a human tumor xenograft. Cancer Res 54:3352–3356